Lithos 356–357 (2020) 105395

Contents lists available at ScienceDirect

Lithos

journal homepage: www.elsevier.com/locate/lithos

Research Article

Early Paleozoic S-type granites as the basement of Southern Qiantang Terrane, Tibet

Wei Dan [a,b,*], Qiang Wang [a,b,c], Xiu-Zheng Zhang [a], Gong-Jian Tang [a,b]

[a] State Key Laboratory of Isotope Geochemistry, Guangzhou Institute of Geochemistry, Chinese Academy of Sciences, Guangzhou 510640, China
[b] CAS Center for Excellence in Tibetan Plateau Earth Science, Beijing 100101, China
[c] College of Earth and Planetary Sciences, University of Chinese Academy of Sciences, Beijing 100049, China

ARTICLE INFO

Article history:
Received 23 October 2019
Received in revised form 20 January 2020
Accepted 20 January 2020
Available online 23 January 2020

Keywords:
Microcontinent
Early Paleozoic
S-type granites
Qiangtang
Cimmeria

ABSTRACT

Identifying basement rocks is critical to understanding the continent formation and evolution during orogenesis. Despite two decades of research, the age and composition of the basement rocks of the Southern Qiangtang Terrane/Microcontinent (SQT), Central Tibet are still unclear. In this study, zircon U–Pb ages and Hf–O isotopes, as well as whole-rock Nd isotopes are presented for the oldest known igneous rocks in the SQT. Precise SIMS zircon U–Pb dating of these rocks reveals that these early Paleozoic granites were crystallized at ca. 480-465 Ma. They exhibit a wide range of isotopic values, with unradiogenic whole rock $\varepsilon_{Nd}(t)$ and zircon $\varepsilon_{Hf}(t)$ values ranging between −8.3~−7.7 and −8.2~−2.3, respectively, and by high $\delta^{18}O_{zircon}$ values of +8.1~+11.4‰. These results reveal that the early Paleozoic granites were crystallized from magmas that were almost entirely sediment-derived. When viewed in concert with regional data and constraints on the tectonic evolution of northern Gondwana, the sources for the early Paleozoic granites are herein proposed to have been deposited in an extensional basin, implying that these early Paleozoic granites were generated in an extensional setting within an accretionary orogen. Thus, the early Paleozoic granites are considered to represent the basement of the SQT. After a long period of attachment to northern Gondwana, the SQT became a small microcontinent when it was rifted and detached from northern Gondwana during Early Permian. After this time, it drifted northwards to Asia, and collided with the Northern Qiangtang Terrane to form a unified Qiangtang terrane in the Late Triassic. Thus, the SQT records a complete Wilson cycle from construction, rifting and departure, drifting to collision.

1. Introduction

Recognition of the basement rocks is critical to understanding the continent formation and evolution, especially for small-scale microcontinents during orogenic events. Microcontinents are typically relatively ribbons of continental crust surrounded by oceanic crust (Scrutton, 1976), and are widely distributed in modern oceans (Tetreault and Buiter, 2014). However, the basement of most modern microcontinents is rarely exposed, hampering investigations into their origin and evolution. Ancient microcontinents, on the other hand, are typically involved in younger orogens when they become accreted to continental margins. Uplift and erosion associated with accretionary processes may expose basement rocks, thereby providing the opportunity to examine a complete Wilson cycle from basement construction, to rift-drift processes, subduction and accretionary orogenic processes (e.g., Murphy et al., 2019). However, basements to microcontinents are typically covered by thick sequences of sedimentary rocks, and, as their provenances are often unclear, are commonly called terranes. Thus, isotopic investigations of sporadic outcrops of the oldest rocks exposed are important to identify the age and characteristics of the microcontinents' basements and therefore their provenances.

The Cimmerian microcontinent, one of the most important terranes in the Tethys realm, separated the Paleo-Tethys from Neo-Tethys, and records the tectonic evolution of the Neo-Tethyan Ocean from its birth to its demise (Şengör, 1979). The Southern Qiangtang Terrane (SQT), Tibet, an important component of the east Cimmerian microcontinent, is covered by Permo-Carboniferous and younger sedimentary rocks. It is well documented that the SQT was detached from northern Gondwana in the Permian (e.g., Zhai et al., 2013a) and was accreted to the Northern Qiangtang Terrane (NQT) in the Late Triassic (e.g., Dan et al., 2018a; Zhai et al., 2011). However, the processes of construction and formation of the proto-SQT are less certain, i.e., the growth and evolution of the SQT before its departure from northern Gondwana. Ordovician magmatism is one of the most important events occurred in the SQT. Thus, understanding the petrogenesis and tectonic setting of these early Paleozoic rocks is key to reveal the composition of its basement and therefore the construction and evolution of the proto-SQT.

In this study, we report lithogeochemical analyses, whole-rock Nd isotopic ratios, and in situ SIMS zircon U–Pb ages and O–Hf isotopic

* Corresponding author.
E-mail address: danwei@gig.ac.cn (W. Dan).

https://doi.org/10.1016/j.lithos.2020.105395
0024-4937/

data for the oldest igneous rocks (early Paleozoic granites) in the SQT, Tibet, western China. These new data are used to constrain the magma source and petrogenesis of the Ordovician granites, and are combined with the regional tectonic constraints on the evolution of northern Gondwana to provide insights into the tectonic setting of the Ordovician magmatism and the age and composition of the basement of the SQT.

2. Geological setting

The Tibetan Plateau exposes a composite orogen comprised of several continental blocks and intervening Tethyan suture zones which range from Paleozoic to Cenozoic in age (Fig. 1a) (Yin and Harrison, 2000). The Longmu Co-Shuanghu suture (LSS) divides the Qiangtang terrane into the NQT and SQT. Although a underthrust model has been proposed (Kapp et al., 2000; Pullen et al., 2011), most studies agree that the LSS is a vestige of the main Paleo-Tethyan Ocean (e.g., Li et al., 1995), evidenced by late Paleozoic magmatic arc and ophiolitic rocks (Dan et al., 2018b, 2019; Zhai et al., 2013b; Zhang et al., 2016) and by Late Triassic blueschists and eclogites (Dan et al., 2018a; Zhai et al., 2011; Zhang et al., 2006a, 2006b, 2018). Silurian high-pressure granulites (~422 Ma) in the LSS indicate that the Paleo-Tethyan Ocean in Tibet opened after ~422 Ma and probably during the Devonian (Dan et al., 2018b, 2019; Zhang et al., 2014, 2016), although the ages of some ophiolites in this suture are Cambrian (Zhai et al., 2016). Widespread deposition of marine sediments in a passive environment followed through the Early Permian in the SQT (Li et al., 1995; Zhang et al., 2013). Widely-distributed Early Permian mafic dike swarms are part of a Permian large igneous province in northern Gondwana, signifying the SQT along with the rest of the Cimmerian continental fragment rifted and detached from northern Gondwana (Xu et al., 2016; Zhai et al., 2013a). Subsequently, the SQT migrated northwards and defined the southern flank of the Paleo-Tethyan Ocean until it collided with the NQT in the Late Triassic (Dan et al., 2018a).

The oldest rocks in the SQT are exposed in the central metamorphic belt, located along its northern margin, which mainly consists of early Paleozoic low-grade and late Paleozoic high-pressure metamorphic rocks and a few early Paleozoic gneissic granites (Li, 2008; Li et al., 1995). The Cambrian low-grade metamorphic quartz sandstones are disconformity overlain by the Middle-Upper Ordovician basal conglomerates and quartz sandstones (Wu et al., 2018; Yang et al., 2014; Zhao et al., 2014). Detrital zircon data display prominent peaks of ~570-550 Ma, ~980-950 Ma and ~2500 Ma, suggesting they were sourced from the Gondwanan continent (Liu et al., 2016a; Pullen et al., 2011; Wu et al., 2018; Xie et al., 2017; Yang et al., 2014; Zhao et al., 2014). Available ages dated by less accurate LA-ICP-MS zircon U–Pb method indicate that early Paleozoic (~500-470 Ma) gneissic granites intruded Cambrian strata (Hu et al., 2015; Liu et al., 2016b; Peng et al., 2014; Pullen et al., 2011; Zhao et al., 2014). Middle Ordovician bimodal volcanism documented in Ordovician strata likely reflects an extensional setting for the Ordovician magmatism (Xie et al., 2017).

Early Paleozoic gneissic granites are mostly exposed in the Duguer and Bengsong Co areas (Fig. 1b). Gneissic granites were emplaced into Cambrian metasedimentary rocks in the Duguer area (Fig. 2a), but are exposed within the Triassic Bengsong Co batholith in the Bengsong Co area (Figs. 1b and 2c). Similar to contemporary rocks in the Himalayas (Gao et al., 2019), these rocks were interpreted to have been mostly derived from metasedimentary rocks with a few mantle-derived melts (Hu et al., 2015). The granites in the both areas are composed mainly of quartz, K-feldspar, plagioclase, muscovite, and minor biotite (Figs. 2b and d). The Duguer granites exhibit porphyritic texture with large phenocrysts of K-feldspar and quartz with minor biotite (<2 vol.%). In contrast, the Bengsong Co granites exhibit coarse granitic texture and have a relatively minor abundance of biotite (2-6 vol.%).

3. Analytical methods

All analyses, including whole rock geochemistry and in-situ zircon U-Pb-O-Hf isotopes were conducted at the State Key Laboratory of Isotope Geochemistry, Guangzhou Institute of Geochemistry, Chinese Academy of Sciences (SKLaBIG GIGCAS). Zircon U–Pb dating and O isotope analyses were conducted by using the Cameca IMS-1280 HR SIMS, and the analytical procedures followed are described by Li et al., 2009; Li et al., 2010a. U-Th-Pb ratios were determined relative to the ~337 Ma standard zircon Plešovice (Sláma et al., 2008). The measured oxygen isotopic data were corrected for instrumental mass fractionation using the Penglai zircon standard ($\delta^{18}O = 5.3‰$) relative to Vienna Standard Mean Ocean Water compositions (VSMOW: $^{18}O/^{16}O = 0.0020052$)

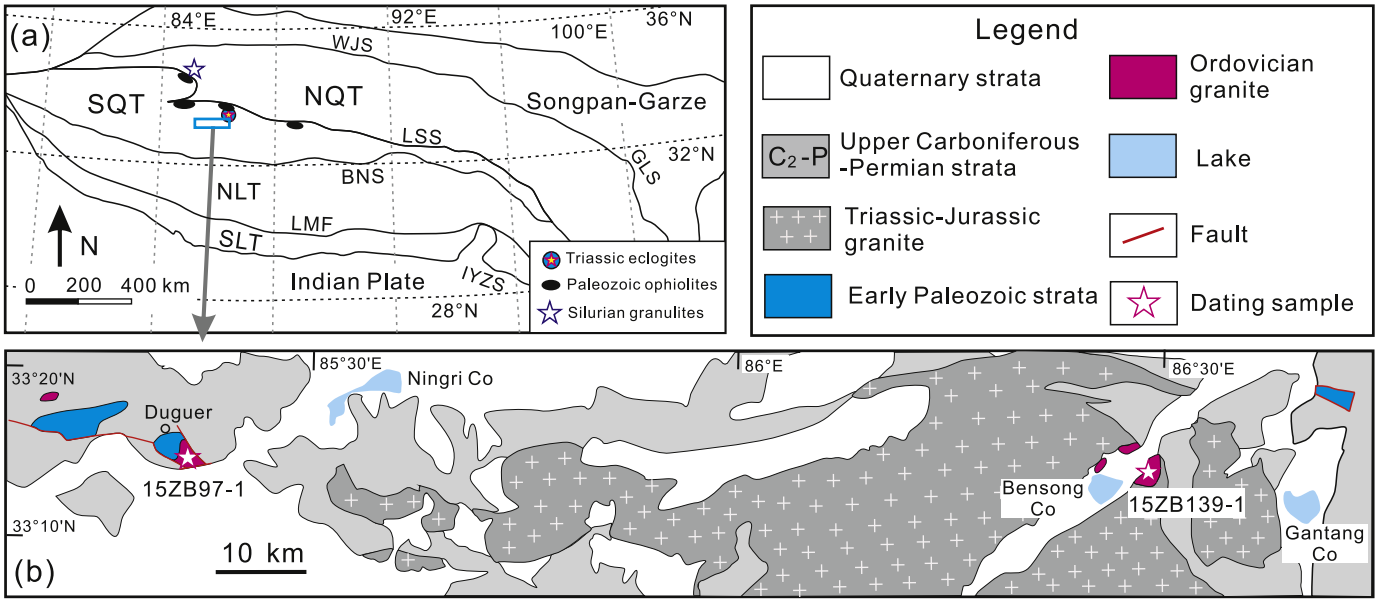

Fig. 1. (a) Tectonic framework of the Tibetan Plateau. Terranes: NQT, Northern Qiangtang Terrane; SQT, Southern Qiangtang Terrane. Sutures: BNS, Bangong-Nujiang suture; GLS, Garze-Litang suture; IYZS, Indus-Yarlung Zangbo suture; LSS, Longmu Co-Shuanghu suture; WJS, West Jinsha suture. (b) Geological map of the Duguer-Gantang Co area in the SQT (modified from Pullen et al., 2011; Liu et al., 2016b and based on our observation), highlighting the early Paleozoic rocks.

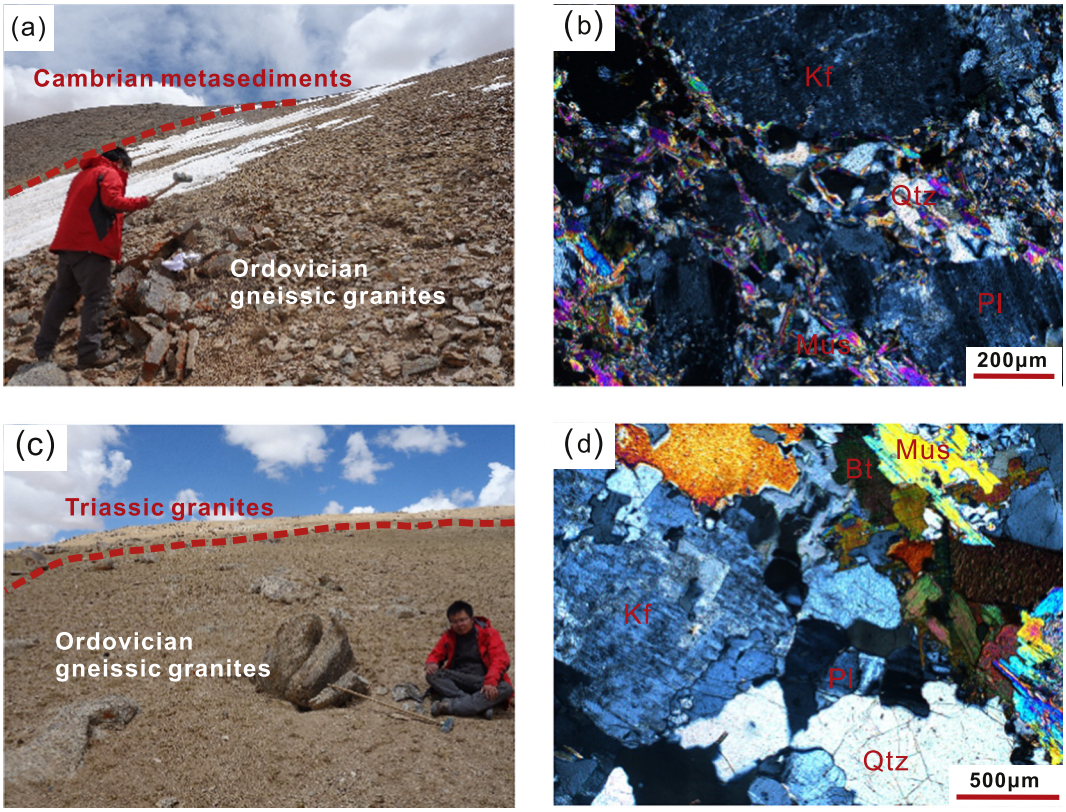

Fig. 2. Field photos and photomicrographs showing field occurrences and mineral assemblages for the Duguer (a–b) and Besong Co (c–d) gneissic granites. Mineral abbreviations: Bt, biotite; Kf, K-feldspar; Mus, Muscovite; Pl, plagioclase; Qtz, quartz.

(Li et al., 2010a). Eleven measurements of the Qinghu zircon standard during the analytical session yielded weighted mean $\delta^{18}O$ of 5.56 ± 0.38‰ (2SD), consistent within errors to the reported value of 5.4 ± 0.2‰ (2SD) (Li et al., 2013).

In-situ zircon Hf isotopes were analyzed by a Neptune Plus multi-collector ICP-MS equipped with a 193-nm (ArF) Resonetics RESOlution M-50 laser-ablation system. Detailed analytical procedures are similar to those described by Zhang et al. (2015). Measured $^{176}Hf/^{177}Hf$ ratios were normalized to $^{179}Hf/^{177}Hf = 0.7325$. Further external adjustment was not applied to the unknowns because our $^{176}Hf/^{177}Hf$ ratios determined for the zircon standards Penglai (0.282906 ± 0.000038, 2SD) and Qinghu (0.282995 ± 0.000026, 2SD) were in good agreement within errors with the reported values (Li et al., 2010a, 2013).

Major element oxides were analyzed on fused glass beads using a Rigaku RIX 2000 X-ray fluorescence spectrometer. Trace elements were analyzed using an Agilent 7500a ICP-MS. Analytical procedures were similar to those described by Li et al. (2000), and the analytical precision is typically better than 5%. Nd isotopic compositions were determined using a Micromass Isoprobe multi-collector ICP-MS. Analytical procedures are similar to those described in Li et al. (2004). All measured Nd isotope ratios were normalized to $^{146}Nd/^{144}Nd = 0.7219$. The measured $^{143}Nd/^{144}Nd$ ratio of the JNdi-1 standard was 0.512105 ± 0.000014 ($n = 20$, 2SD).

4. Results

4.1. Zircon U–Pb dating

Zircon grains from two gneissic granites are mostly euhedral to subhedral, ~100-150 μm or less in length, with length to width ratios of 2:1 to 3:1 (Fig. 3). Almost all grains show oscillatory zoning in cathodoluminescence images, indicative of their magmatic origin. All analyzed grains have moderate Th (47-125 ppm) and U (138-870 ppm) contents, with Th/U rations of 0.10-0.23 (Table A.1).

U–Pb concordia diagrams of analyzed zircons are shown in Fig. 3. Fourteen grains from sample 15ZB97-1 (Duguer granite) have $^{206}Pb/^{238}U$ dates ranging from 456 to 475 Ma, with a weighted mean age of 465 ± 4 Ma. In sample 15ZB139-1 (Bensong Co granite), two zircon grains yielded older $^{207}Pb/^{206}Pb$ dates of ~1.9-1.7 Ga. All 13 grains from sample 15ZB139-1 define a lower intercept at 477 ± 9 Ma, indicating that the older grains underwent Pb loss during the Ordovician magmatism. The two older zircon grains have no obvious younger crystallized rims (Fig. 3), thus, they are interpreted as xenocrysts. Ten zircon grains have $^{206}Pb/^{238}U$ dates from 469 to 491 Ma, with a weighted mean age of 480 ± 4 Ma. One grain is discordant with a younger $^{206}Pb/^{238}U$ date of 453 Ma, which was interpreted to be an artefact of later Pb loss.

Early Paleozoic granites in the SQT were previously considered to by Late Cambrian-Middle Ordovician in age (Hu et al., 2015; Liu et al., 2016b; Peng et al., 2014; Pullen et al., 2011; Zhao et al., 2014), on the basis of less accurate LA-ICP-MS zircon U–Pb dating method (Li et al., 2015). For example, Bensong Co and Duguer granites were previously dated to 497-481 Ma and 485-471 Ma, respectively (Hu et al., 2015; Peng et al., 2014; Pullen et al., 2011). However, the more accurate SIMS zircon U–Pb dating method employed in this study shows that the Bensong Co and Duguer granites were formed at 480 Ma and 465 Ma, respectively. Thus, these new ages will be used in the following discussion.

4.2. Zircon O–Hf isotopic compositions

Measured $\delta^{18}O_{zircon}$ values for sample 15ZB97-1 exhibit a wide range (8.1–10.9‰) (Table A.2), with a major peak at 10.4‰ (Fig. 4a). Most zircon grains from sample 15ZB139-1 have $\delta^{18}O_{zircon}$ values of 10.5–11.4‰, with one slightly lower value of 9.3‰ (Fig. 4b). Two

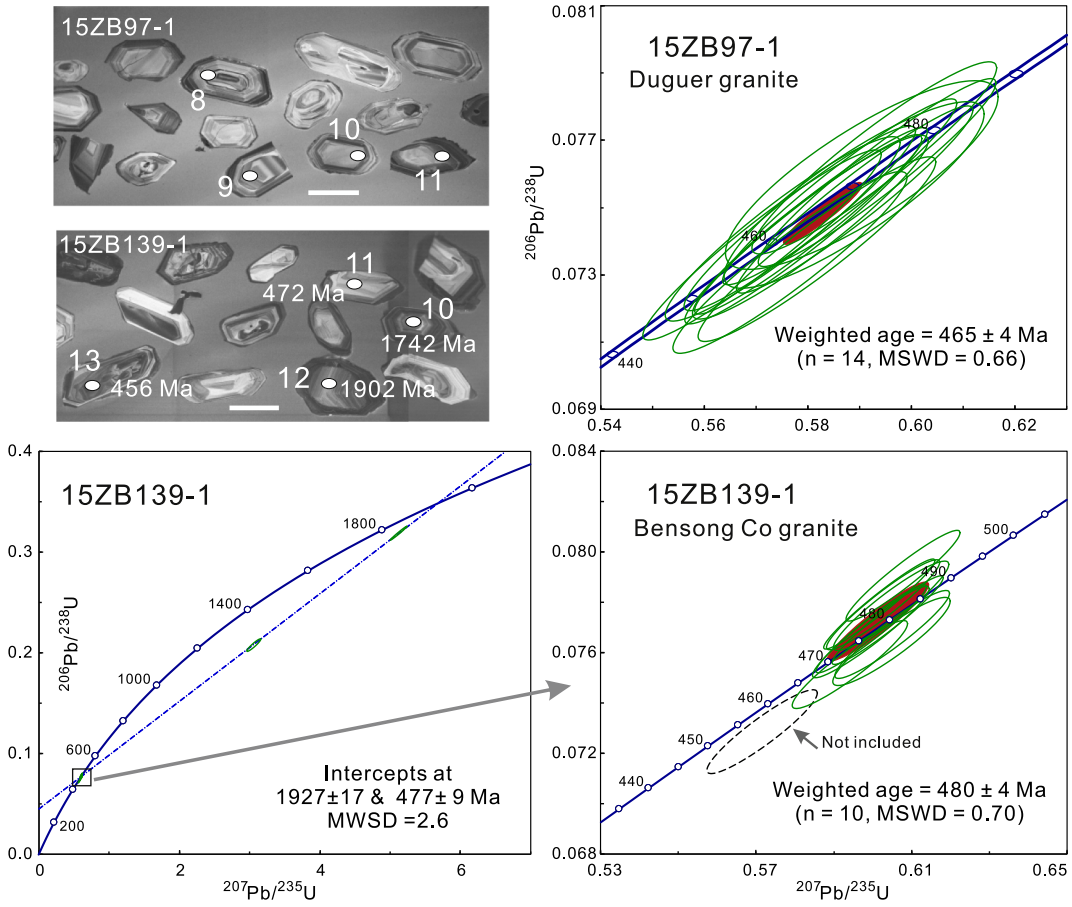

Fig. 3. Cathodoluminescence (CL) images of zircons and SIMS zircon U–Pb ages for Ordovician granites in the SQT. Numbers near the analysis spots in CL images from 15ZB139-1 are the U–Pb dates (Ma). The white scale bars in CL images are 100 μm long.

analyses of dated xenocrystic zircon grains yield different $\delta^{18}O_{zircon}$ values (10.7‰ and 6.5‰).

Twenty-five zircon grains from sample 15ZB97-1 have a limited range in initial $^{176}Hf/^{177}Hf$ isotopic ratios of 0.282252-0.282371, corresponding to $\varepsilon_{Hf}(t)$ values ranging between −8.2 to −3.9 (Fig. 4c), with an average of −5.4 ± 2.1 (2SD). Twenty-four zircon grains from sample 15ZB139-1 have a wider range of $^{176}Hf/^{177}Hf$ ratios of 0.281453–0.282424. The xenocrystic grains have pronounced lower $^{176}Hf/^{177}Hf$ isotopic ratios of 0.281453–0.281792 compared to the ~480 Ma grains of 0.282299–0.282424. One undated grain (spot 19) with low $^{176}Hf/^{177}Hf$ isotopic ratios of 0.282208 is ascribed to a xenocrystic origin. Thus, the remaining 21 grains with ~480 Ma have $\varepsilon_{Hf}(t)$ values of −6.8 to −2.3 (Fig. 4c), averaging at −4.2 ± 1.9 (2SD). In addition, the zircon $\varepsilon_{Hf}(t)$ values do not show obvious covariation with the O isotopes (Fig. 4d).

4.3. Whole-rock geochemistry and Nd isotopes

The Ordovician granites, including samples from Hu et al. (2015), have high K_2O contents (3.66-6.92 wt.%) (Table A.3), and are classified as high-K calc-alkaline series (Fig. 5a). They have high A/CNK (molar $Al_2O_3/(CaO + Na_2O + K_2O)$) >1.1 and so have peraluminous compositions (Fig. 5b). Almost all samples show enrichment in light rare earth elements (LREEs), depletion in high field-strength elements (HFSEs, e.g., Nb, Ta, and Ti) (Figs. 5c-d), and pronounced negative Eu anomalies. Sample 15ZB139-1 shows a positive Eu anomaly and has the lowest SiO_2, indicating a possible cumulative origin.

Five samples were analyzed for whole-rock Nd isotopes (Table A.4). Four samples show similar $\varepsilon_{Nd}(t)$ values ranging from −8.3~−7.7. The cumulative sample of 15ZB139-1 has a slightly higher $\varepsilon_{Nd}(t)$ values of -6.4 (Fig. 5f). However, two anomalous samples with higher $\varepsilon_{Nd}(t)$ values of -3.7 and +0.5 obtained by Hu et al. (2015) were excluded from this study with explanation given below.

5. Discussion

5.1. Sediment-derived Ordovician granites in the SQT

Previous whole-rock geochemical studies have demonstrated that the Ordovician granites in the SQT were mainly derived from partial melting of metasedimentary rocks (Hu et al., 2015). These granites have low whole rock $\varepsilon_{Nd}(t)$ values of −8.3~−6.4, and negative zircon $\varepsilon_{Hf}(t)$ values of −4.2 to −5.6 (this study and Hu et al., 2015), further emphasizing that they were sourced from ancient crustal materials. Based on two anomalous higher $\varepsilon_{Nd}(t)$ values of −3.7 and +0.5, minor amounts of mantle-derived components were proposed to be introduced into their magma sources (Hu et al., 2015). However, the samples with higher $\varepsilon_{Nd}(t)$ values have similar zircon $\varepsilon_{Hf}(t)$ values to other samples with low $\varepsilon_{Nd}(t)$ values. Furthermore, their Rb and Sr concentration and Rb/Sr ratios (<1) are strikingly different from those with normal values which have high Rb/Sr ratios (>7) (Table A.4). Thus, the two anomalous samples cannot be used to discuss the petrogenesis of Ordovician granites without further studies.

Previous studies demonstrate that in-situ zircon Hf–O isotopes can effectively recognize the potential sources of granites. The predominantly sediment-derived granites are characterized by a wide range of high zircon O isotopes ($\delta^{18}O_{zircon}$ >8‰) and no correlation between zircon O and Hf isotopic values (Dan et al., 2014a; Hopkinson et al., 2017). In contrast, S-type granites with some meta-igneous components or mantle-derived melts involved in their generation have a wide range

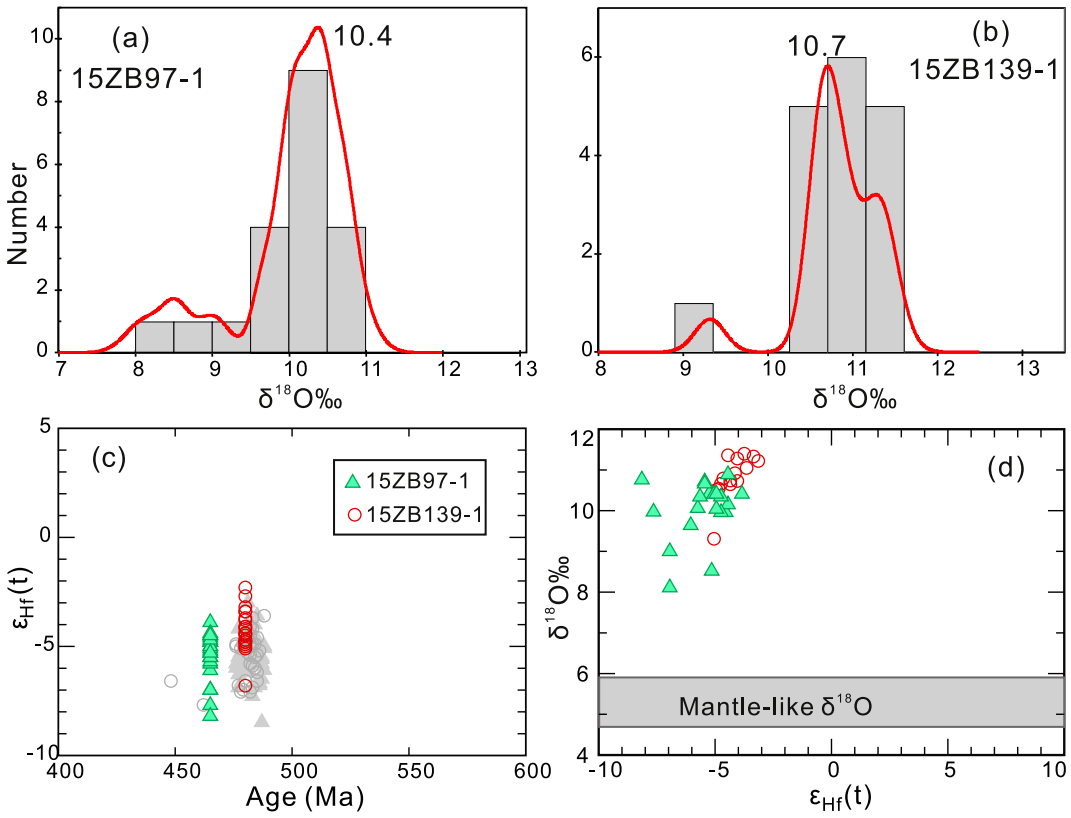

Fig. 4. In-situ zircon O and Hf isotopes for Ordovician granites in the SQT. Grey symbols in (c) are from Hu et al. (2015), and the $\delta^{18}O_{zircon}$ values of depleted-mantle in (d) (Valley et al., 1998) are shown for comparison.

of $\delta^{18}O_{zircon}$, but some zircons have values <8‰, and, in general are characterized by a negative relationship between zircon O and Hf isotopes (Appleby et al., 2010; Dan et al., 2014b; Li et al., 2009b). The Ordovician granites have high $\delta^{18}O_{zircon}$ values (from 8.1 to 11.4‰), corresponding to whole rock $\delta^{18}O$ values of 10.1 to 13.3‰, based on the relationship between $\delta^{18}O_{zircon}$ values and granitic melt (Lackey et al., 2008). The high $\delta^{18}O_{W.R.}$ values (>10‰), together with the lack of covariation between zircon Hf and O isotopes (Fig. 4d), suggest these granites were produced predominantly by partial melting of metasedimentary rocks (Dan et al., 2014a; O'Neil and Chappell, 1977). In addition, the granites have high zircon saturation temperatures (~700–900 °C, Fig. 5e) suggesting that their sources underwent fluid-absent muscovite/biotite dehydration melting, rather than low temperature fluid-present melting (Brown, 2013; Zeng and Gao, 2017). Their high Rb/Sr ratios, which increase with decreasing Ba and Sr contents (Fig. 6), further suggest that they were derived from fluid-absent muscovite dehydration melting of metasedimentary rocks (Inger and Harris, 1993).

5.2. Tectonic setting of the Ordovician magmatism

Numerous early Paleozoic (~540–460 Ma) magmatic rocks have been identified along the northern Gondwana margin and were proposed to be related to subducted-related orogeny (e.g., Cawood et al., 2007; Li et al., 2018; Zhu et al., 2012), although a passive margin environment has been proposed for the northern Gondwana margin from late Cambrian (Miller et al., 2001). Different models have been proposed for the tectonic setting of the Ordovician magmatism in northern Gondwana, including backarc extension related to accretionary orogenesis (Wang et al., 2013), slab break-off (Hu et al., 2015) and lithospheric detachment (Li et al., 2016; Liu et al., 2016b).

Although it is hard to distinguish between these mechanisms, there are several features that can help to decipher the tectonic setting of the Ordovician magmatism. It is noteworthy that the Cambrian-Ordovician unconformity is prevalent along the northern Gondwana margin and in the peri-Gondwanan terranes (Lhasa, SQT and Baoshan) (Cawood et al., 2007; Huang et al., 2009; Li et al., 2010b). This unconformity was probably related to an extensional event rather than collisional orogeny, because the angular unconformity is confined to Himalaya and Lhasa terranes and in most areas the unconformity is a disconformity (Liu et al., 2016b; Zhou et al., 2004). During the Ordovician, the Proto-Tethyan Ocean outside the realm of the SQT remained open and is characterized by Cambrian-Ordovician ophiolites (Zhai et al., 2016) in the central Qiangtang. Ordovician magmatism in the peri-Gondwanan terranes (SQT, Baoshan-Sibumasu, Tengchong and Lhasa) is characterized by S-type granites and minor mafic rocks and an absence of I-type granites (Wang et al., 2013; Hu et al., 2015; this study). These features cannot be ascribed to either slab break-off or lithospheric detachment, which will generate various types of granites and mafic rocks (e.g., Dan et al., 2014b; Garzanti et al., 2018). Thus, we maintain that the Ordovician and even Cambrian magmatism was generated in an extensional setting (e.g., Liu et al., 2016b; Miller et al., 2001; Xie et al., 2017), and that a backarc extensional setting (e.g., Wang et al., 2013) is more consistent with regional constraints than other models.

A backarc extension setting was first proposed by Wang Y.J. et al. (2013) to explain the early Paleozoic S-type magmatism in SW Yunnan, China, including Baoshan, Tengchong and Sibumasu terranes. This model emphasizes that the source of the S-type granites was deeply buried before anatexis. Combined with arc systems before and after the Ordovician S-type magmatism, the tectonic setting of post-collision S-type magmatism was related to accretionary orogenesis. Its generation was related to anatexis of thickened sedimentary rocks in a pre-existing backarc basin (Wang et al., 2013). This process was proposed for the Tasmanide orogenic system in eastern Australia to explain the voluminous but short-lived S-type magmatism (e.g., Collins and Richards, 2008). In this context, the generation of S-type magmatism involves three processes, i.e., backarc basin

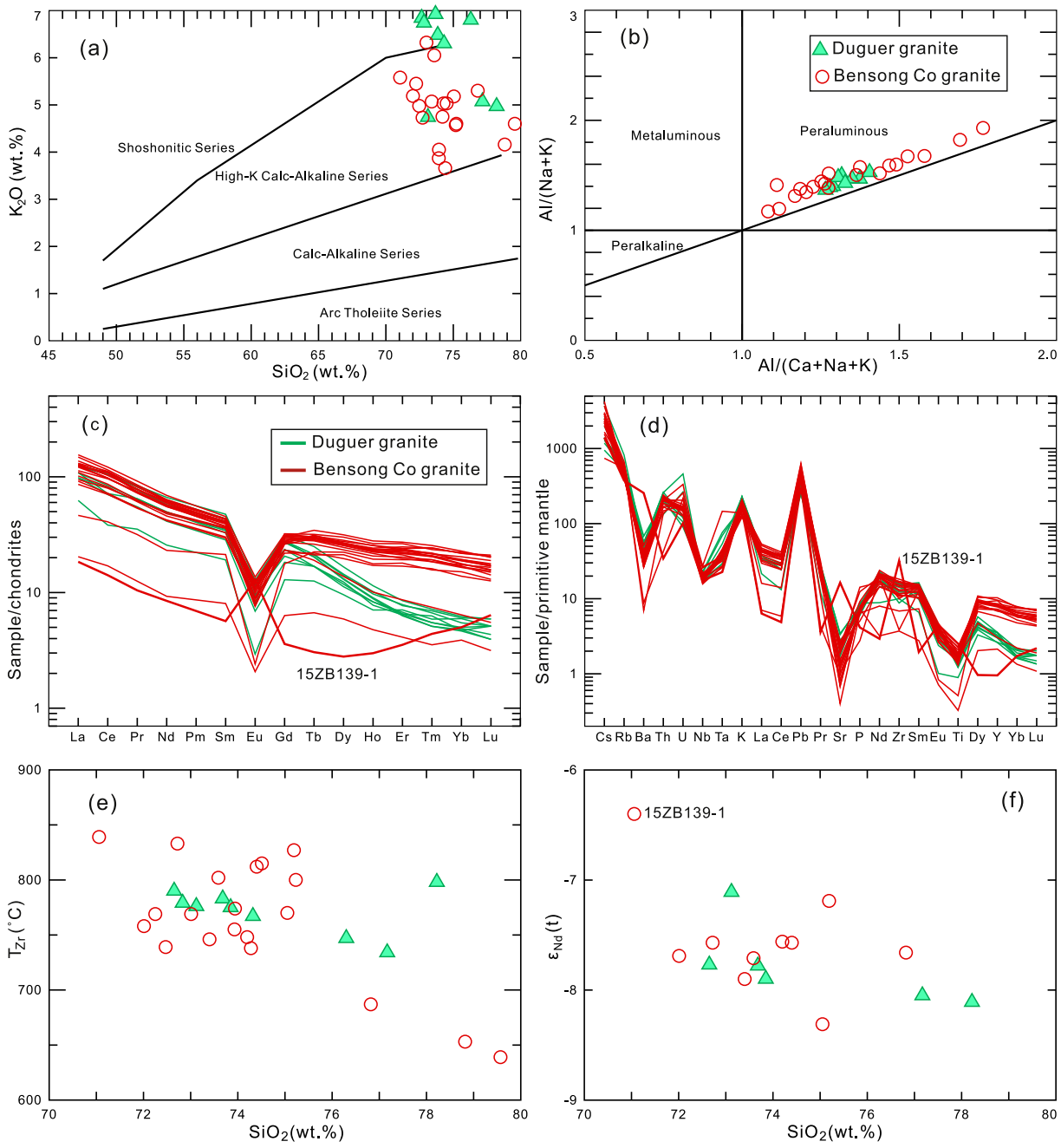

Fig. 5. Geochemistry of the Ordovician granites in the SQT. The normalized data in (c–d) are from Sun and McDonough (1989); Zircon saturation temperatures in (e) are calculated based on Boehnke et al. (2013), and 3 samples with lower temperatures <700 °C but higher SiO_2 are probably results of crystallization differentiation.

formation to deposit sedimentary rocks, followed by closure of the backarc basin to thicken and metamorphosed the sedimentary rocks and then by melting of the thickened backarc crust in a regional extensional setting. The tectonic evolution of early Paleozoic in the SQT is similar to the Baoshan Terrane, and the post-orogenic extension setting applies to the Ordovician magmatism in the SQT (Fig. 7).

Although the backarc model satisfies most of the published data, it doesn't explain all phenomena. For example, there are no I-type granites reported in the ~510-460 Ma interval along the NE Gondwana margin, including in the peri-Gondwanan terranes, such as SQT, Baoshan and Lhasa (e.g., Cawood et al., 2007; Gao et al., 2019; Wang et al., 2013). This implies that subducted-related magmatic arcs, if they existed, were located outside these terranes (Fig. 7). If so, they were either eroded, subducted during subsequent accretionary orogenesis or the magmatic arcs were located in an unknown microcontinent. These anomalies indicate that more studies are required to reveal the tectonic evolution of the NE Gondwana margin.

5.3. Ordovician granites as the SQT basement

Chinese geoscientists have studied the basement of the SQT early to 1980s. The early proposal of a Mesoproterozoic or older basement existing was criticized by Li (2003, 2008) based on regional geology and geochronology. Based on the early Paleozoic strata and ~510-460 Ma magmatism discovered in the SQT, Lhasa and Himalaya terranes, Li (2003, 2008) speculated these terranes have Pan-African basement formed during accretionary orogenesis along northern Gondwanan margin. In recent years, the early Paleozoic low-grade metasedimentary rocks intruded by ~470 Ma granites were considered as the basement by some researchers (Zhao et al., 2014), although a

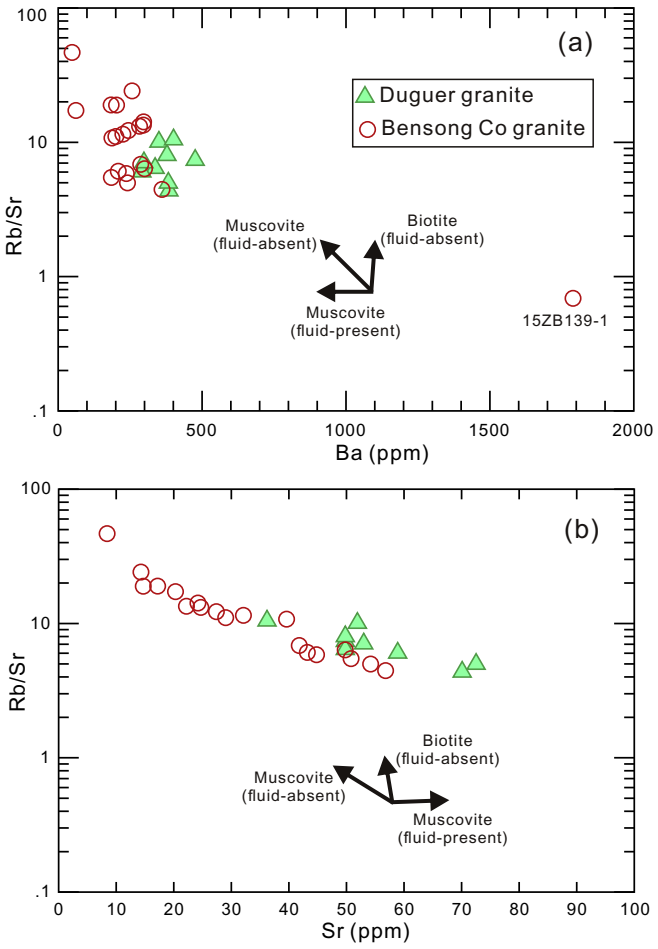

Fig. 6. Large iron lithospheric element covariation for Ordovician granites in the SQT. Small black vectors show different melting trends dominated by muscovite/biotite fluid-present or -absent melting (Inger and Harris, 1993).

Paleoproterozoic-aged basement was proposed by some researchers based on Nd and Hf model ages (Hu et al., 2015; Liu et al., 2019).

Recent studies reveal that the Meso- and Neoproterozoic magmatism prevailed in the northern India and Lhasa Terrane (Hu et al., 2018; Zhang et al., 2012a). However, only Cambrian-Ordovician sedimentary rocks but no Precambrian rocks were discovered in the SQT (Liu et al., 2016a; Zhao et al., 2014), despite intensive studies to identify basement. Detrital zircons with prominent peaks of ~950 Ma and ~570 Ma reveal these sedimentary rocks were sourced from the Gondwana continent (Liu et al., 2016a). These data indicate that the metasedimentary rocks in the SQT were derived from the main continent of the Gondwana, and not from any sources within the SQT itself. As the Ordovician granites are only slightly younger than the Cambrian sedimentary rocks, we propose that the Ordovician granites as the basement of the SQT. The Ordovician thermal-tectonic event probably marks the stabilization and cratonization of the SQT segment of Cimmerian microcontinent. After this event, the SQT remained as a stable terrane until the Permian when regional extensive rifted-related magmatism occurred. This scenario is analogous to the Tasmanide orogenic system in east Australia (e.g., Collins and Richards, 2008) where the S-type granites represent the basement of accreted terranes.

The proposal of the SQT with Ordovician basement is partly consistent with the model of previous researchers (Zhao et al., 2014), but we emphasize that the Ordovician granites, not the Cambrian low-grade metasedimentary rocks, represent the basement. The deep crust should also consist of these igneous rocks and high-grade metasedimentary rocks, which were deposited in an extensional basin with no or thin continental crust. Alternatively, older lower crust was delaminated during the Late Triassic post-collisional period after the collision between SQT and NQT (Dan et al., 2018a) or became detached during younger Mesozoic subduction along the Bangong-Nujiang suture beneath SQT (e.g., Zhang et al., 2017a). Furthermore, the prevalence of sediment-derived Ordovician granites with no I-type granites discovered in the SQT suggests that their Paleoproterozoic Nd or Hf model ages cannot used to indicate the age of ancient basement in the SQT, although the possibility of that minor older basement exists in some areas cannot be totally excluded.

It is noteworthy that other east Cimmerian terranes have a similar early Paleozoic evolution to the SQT. The oldest rocks discovered in the Baoshan-Sibumasu Terrane, the SE extension of the SQT, are Cambrian-Ordovician sedimentary rocks, which have unconformity within this succession and are intruded by many S-type granites (e.g., Huang et al., 2009; Lin et al., 2013). Thus, this terrane was also stabilized and cratonized during the early Paleozoic tectonic-magmatic event. In contrast, Neoproterozoic magmatism and metamorphism prevailed in Northern Lhasa (Hu et al., 2018; Zhang et al., 2012a), although this terrane exposes a similar early Paleozoic evolution to the SQT (e.g., Zhu et al., 2012). Thus, the Northern Lhasa Terrane has an older basement and different origin from other east Cimmerian terranes.

5.4. Microcontinent origin for the SQT

The tectonic evolution framework of the Qiangtang terrane is highly debated, and two incompatible models, i.e., in-situ suture zone and an underthrusted zone, have been proposed. The in-situ suture model maintains that the LSS represents an in-situ Paleo-Tethys suture,

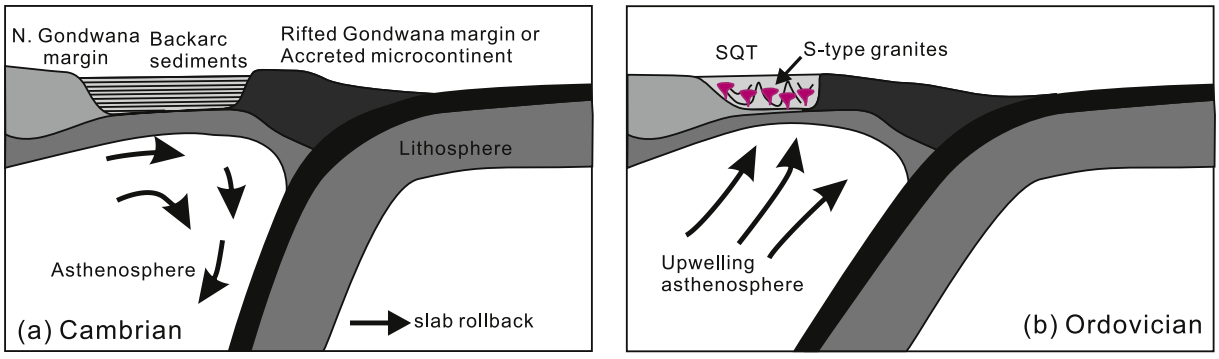

Fig. 7. Cartoon illustrating the evolution of the SQT (microcontinent) from construction, generation to accretion/collision (modified from Collins and Richards, 2008; Wang et al., 2013). (a) The northern Gondwana margin underwent strong extension forming an oceanic backarc basin at Cambrian during slab rollback or an extensional basin formed behind an unknown accreted microcontinent; (b) The former backarc sediments underwent melting to form S-type granites at Ordovician or older during post-orogenic extension.

separating the SQT from the NQT (e.g., Li, 1987, 2008; Li et al., 1995). This model is adopted by most researchers and is consistent with the discovery of late Paleozoic ophiolites, magmatic arc and Late Triassic eclogites (e.g., Dan et al., 2018a; Zhai et al., 2011; Zhang et al., 2006a). The underthrust model considers the Qiangtang terrane is a single terrane that was detached from Gondwana continent, and the central metamorphic belt in central Qiangtang is a tectonic mélange underplated through low-angle southward subduction in Jinsha suture beneath the Qiangtang terrane during the Middle Triassic (Kapp et al., 2000; Pullen et al., 2011). Recently, the similar detrital zircon patterns between south and north sides of the central metamorphic belt, previously thought represent SQT and NQT, respectively, and glaciomarine diamictites in Carboniferous–early Permian strata occurring on the north side of the central metamorphic belt (Gehrels et al., 2011) were taken to support the underthrust model (Pullen and Kapp, 2014). However, the location of the LSS was refined by recent studies in Permian ophiolites (Zhang et al., 2016), Devonian-Carboniferous magmatic arc rocks (Dan et al., 2018b, 2019; Jiang et al., 2015) and early Paleozoic strata (Wu et al., 2018) to north of the central metamorphic belt. Thus, previous sample thought to have been located in the NQT (Gehrels et al., 2011) are actually located in the SQT. This suggestion is consistent with those Carboniferous-Permian samples lacking the late Paleozoic detrital zircon populations that characterize Carboniferous or younger strata in the NQT (Zhang et al., 2017b).

Our data are consistent with in-situ suture model, although the central metamorphic belt was sometimes considered as an accretionary complex (Liang et al., 2012, 2017), and the southern younger Permian-Cenozoic strata as the SQT. This accretionary complex was thought to include the Ordovician rocks, Permian sedimentary rocks and high-pressure metamorphic rocks, ophiolite relics, and rift-related mafic dyke swarms (Liang et al., 2012, 2017). However, stratigraphic and fossil studies reveal most strata in the central metamorphic belt have Gondwanan affinity, and that Permian strata are related to the rifting and detachment of the SQT from the Gondwana continent (Zhang et al., 2012b). Thus, the accretionary complex, if existed, may be confined to a small area such as the studied Qomo Ri area (Liang et al., 2012, 2017).

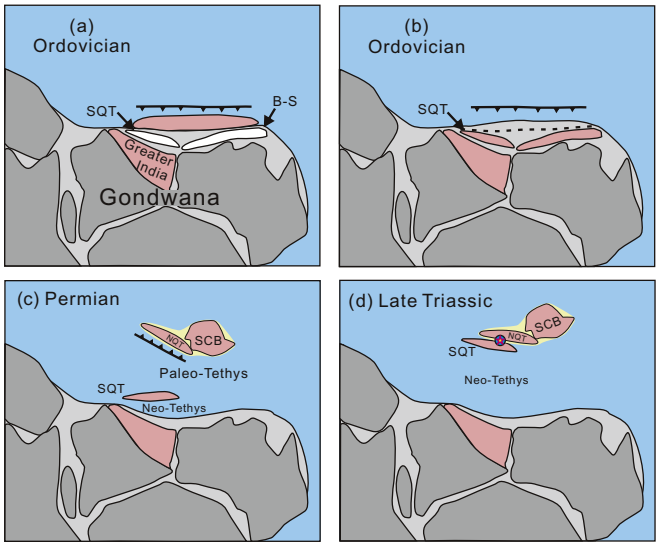

Fig. 8. Cartoon illustrating the SQT (microcontinent) from construction, rifting to accretion/collision (modified from Zhai et al., 2013a; Dan et al., 2018b). (a–b) The SQT was constructed and cratonized during the Ordovician behind an unknown microcontinent or the rifted Gondwana continent margin; (c) The SQT was rifted from northern Gondwana margin and drifted to the NQT during Permian; (d) The SQT collided with NQT during the Late Triassic. Other terranes were omitted in (c–d) to highlight the evolution of the SQT. B–S, Baoshan-Sibumasu; SCB, South China Block. The symbol of star in (d) indicates eclogites.

The in-situ model implies that SQT is a microcontinent, one segment of the Cimmerian microcontinent, that became detached from the Gondwana continent in Permian (Zhai et al., 2013a). The SQT records a whole cycle of a microcontinent's evolution including its construction, rifting and drifting, to accretion/collision (Fig. 8). In the early Paleozoic, the proto-SQT would have been located along a subducted-related continental margin, possibly as a basin, and its basement was generated during the Ordovician magmatism. This event and/or later Silurian orogeny stabilized and cratonized this area. During the Permian, the area was rifted and detachment from the Gondwana continent as a small microcontinent, i.e., SQT. During drifting northwards to Asia, the regional extent of the SQT expanded because of younger deposition and/or accretionary process along its southern side (e.g., Zhang et al., 2017a). In the Late Triassic, the SQT collided with the NQT forming a unified Qiangtang terrane.

6. Conclusions

New SIMS zircon U–Pb dating confirms that the early Paleozoic granites in the Southern Qiangtang Terrane were formed at 480-465 Ma. The unradiogenic Hf and Nd isotopes and high zircon O isotopes imply that the early Paleozoic granites were crystallized from melts that were almost sediment-derived. These sediments were likely deposited in an extensional setting during regional accretionary orogenesis. An early Paleozoic tectonic-magmatic event cratonized this area and constructed the basement of proto-Southern Qiangtang Terrane, which was detached from the Gondwana continent during the Early Permian, becoming a small microcontinent. This microcontinent drifted towards Asia and collided with it in the Late Triassic.

Acknowledgments

Constructive comments by Editor-in Chief Prof. Xian-hua Li and two anonymous reviewers substantially improved this manuscript. Prof. J. Brendan Murphy is thanked for proofreading the revised version of this paper. This study was supported by the National Key R & D Program of China (2016YFC0600407), the National Natural Science Foundation of China (Nos. 91855215, 41630208, 41573027, 41673033, 41722205), the Second Tibetan Plateau Scientific Expedition and Research (STEP) (2019QZKK0702), the Key Program of the Chinese Academy of Sciences (QYZDJ-SSW-DQC026), the GIGCAS 135 project 135TP201601, and the Key Program of Guangzhou City (201707020032). This is contribution No.IS-2807 from GIGCAS.

Declaration of Competing Interest

The authors declare that they have no known competing financial interests or personal relationships that could have appeared to influence the work reported in this paper.

Appendix A. Supplementary data

Supplementary data to this article can be found online at https://doi.org/10.1016/j.lithos.2020.105395.

References

Appleby, S.K., Gillespie, M.R., Graham, C.M., Hinton, R.W., Oliver, G.J.H., Kelly, N.M., Eimf, 2010. Do S-type granites commonly sample infracrustal sources? New results from an integrated O, U-Pb and Hf isotope study of zircon. Contributions to Mineralogy and Petrology 160, 115–132.

Boehnke, P., Watson, E.B., Trail, D., Harrison, T.M., Schmitt, A.K., 2013. Zircon saturation re-revisited. Chemical Geology 351, 324–334.

Brown, M., 2013. Granite: From genesis to emplacement. Geological Society of America Bulletin 125, 1079–1113.

Cawood, P.A., Johnson, M.R.W., Nemchin, A.A., 2007. Early Palaeozoic orogenesis along the Indian margin of Gondwana: tectonic response to Gondwana assembly. Earth and Planetary Science Letters 255, 70–84.

Collins, W.J., Richards, S.W., 2008. Geodynamic significance of S-type granites in circum-Pacific orogens. Geology 36, 559–562.

Dan, W., Li, X.H., Wang, Q., Wang, X.C., Liu, Y., 2014a. Neoproterozoic S-type granites in the Alxa Block, westernmost North China and tectonic implications: In situ zircon U-Pb-Hf-O isotopic and geochemical constraints. American Journal of Science 314, 110–153.

Dan, W., Li, X.-H., Wang, Q., Wang, X.-C., Liu, Y., Wyman, D.A., 2014b. Paleoproterozoic S-type granites in the Helanshan Complex, Khondalite Belt, North China Craton: Implications for rapid sediment recycling during slab break-off. Precambrian Research 254, 59–72.

Dan, W., Wang, Q., White, W.M., Zhang, X.-Z., Tang, G.-J., Jiang, Z.-Q., Hao, L.-L., Ou, Q., 2018a. Rapid formation of eclogites during a nearly closed ocean: Revisiting the Pianshishan eclogite in Qiangtang, central Tibetan Plateau. Chemical Geology 477, 112–122.

Dan, W., Wang, Q., Zhang, X.-Z., Zhang, C., Tang, G.-J., Wang, J., Ou, Q., Hao, L.-L., Qi, Y., 2018b. Magmatic record of Late Devonian arc-continent collision in the northern Qiangtang, Tibet: implications for the early evolution of East Paleo-Tethys Ocean. Lithos 308-309, 104–117.

Dan, W., Wang, Q., Li, X.-H., Tang, G.-J., Zhang, C., Zhang, X.-Z., Wang, J., 2019. Low δ18O magmas in the carboniferous intra-oceanic arc, central Tibet: implications for felsic magma generation and oceanic arc accretion. Lithos 326-327, 28–38.

Gao, L.-E., Zeng, L., Hu, G., Wang, Y., Wang, Q., Guo, C., Hou, K., 2019. Early Paleozoic magmatism along the northern margin of East Gondwana. Lithos 334-335, 25–41.

Garzanti, E., Radeff, G., Malusà, M.G., 2018. Slab breakoff: A critical appraisal of a geological theory as applied in space and time. Earth-Sci. Rev. 177, 303–319.

Gehrels, G., Kapp, P., DeCelles, P., Pullen, A., Blakey, R., Weislogel, A., Ding, L., Guynn, J., Martin, A., McQuarrie, N., Yin, A., 2011. Detrital zircon geochronology of pre-Tertiary strata in the Tibetan-Himalayan orogen. Tectonics 30. https://doi.org/10.1029/2011TC002868 TC5016.

Hopkinson, T.N., Harris, N.B.W., Warren, C.J., Spencer, C.J., Roberts, N.M.W., Horstwood, M.S.A., Parrish, R.R., Eimf, 2017. The identification and significance of pure sediment-derived granites. Earth Planet. Sci. Lett. 467, 57–63.

Hu, P.Y., Zhai, Q.G., Jahn, B.M., Wang, J., Li, C., Lee, H.Y., Tang, S.H., 2015. Early Ordovician granites from the South Qiangtang terrane, northern Tibet: implications for the early Paleozoic tectonic evolution along the Gondwanan proto-Tethyan margin. Lithos 220, 318–338.

Hu, P.-y., Zhai, Q.-g., Wang, J., Tang, Y., Wang, H.-t., Hou, K.-j., 2018. Ediacaran magmatism in the North Lhasa terrane, Tibet and its tectonic implications. Precambrian Research 307, 137–154.

Huang, Y., Deng, G.B., Peng, C.L., Hao, J.X., Zhang, G.X., 2009. The discovery and significance of absence in Early–Middle Ordovician in southern Baoshan, western Yunnan. Guizhou Geol. 26, 1–6 (in Chinese with English abstract).

Inger, S., Harris, N., 1993. Geochemical constraints on leucogranite magmatism in the Langtang Valley, Nepal Himalaya. Journal of Petrology 34, 345–368.

Jiang, Q.Y., Li, C., Su, L., Hu, P.Y., Xie, C.M., Wu, H., 2015. Carboniferous arc magmatism in the Qiangtang area, northern Tibet: zircon U-Pb ages, geochemical and Lu-Hf isotopic characteristics, and tectonic implications. Journal of Asian Earth Sciences 100, 132–144.

Kapp, P., Yin, A., Manning, C.E., Murphy, M., Harrison, T.M., Spurlin, M., Lin, D., Deng, X.G., Wu, C.M., 2000. Blueschist-bearing metamorphic core complexes in the Qiangtang block reveal deep crustal structure of northern Tibet. Geology 28, 19–22.

Lackey, J.S., Valley, J.W., Chen, J.H., Stockli, D.F., 2008. Dynamic magma systems, crustal recycling, and alteration in the Central Sierra Nevada Batholith: the oxygen isotope record. Journal of Petrology 49, 1397–1426.

Li, C., 1987. The Longmucuo–Shuanghu–Lancangjiang plate suture and the north boundary of distribution of Gondwana facies Carboniferous–Permian system in northern Xizang, China. J. Changchun Coll. Geol. 17, 155–166 (in Chinese with English Abstract).

Li, C., 2003. Question about the basement of the Qiangtang Micro–Plate. Geol. Rev. 49, 4–9 (in Chinese with English abstract).

Li, C., 2008. A review on 20 year's study of the Longmu Co–Shuanghu–Lancang river suture zone in Qinghai–Xizang (Tibet) Plateau. Geol. Rev. 54, 105–119 (in Chinese with English abstract).

Li, C., Cheng, L.R., Hu, K., Yang, Z.R., Hong, Y.R., 1995. Study on the Paleo-Tethys suture zone of Longmu Co-Shuanghu, Tibet. Geological Publishing House, Beijing (in Chinese with English abstract).

Li, X.H., Sun, M., Wei, G.J., Liu, Y., Lee, C.Y., Malpas, J., 2000. Geochemical and Sm-Nd isotopic study of amphibolites in the Cathaysia Block, southeastern China: evidence for an extremely depleted mantle in the Paleoproterozoic. Precambrian Research 102, 251–262.

Li, X.H., Liu, D.Y., Sun, M., Li, W.X., Liang, X.R., Liu, Y., 2004. Precise Sm-Nd and U-Pb isotopic dating of the supergiant Shizhuyuan polymetallic deposit and its host granite, SE China. Geological Magazine 141, 225–231.

Li, X.-H., Liu, Y., Li, Q.-L., Guo, C.-H., Chamberlain, K.R., 2009a. Precise determination of Phanerozoic zircon Pb/Pb age by multicollector SIMS without external standardization. Geochemistry, Geophysics, Geosystems 10. https://doi.org/10.1029/2009GC002400.

Li, X., Li, W., Wang, X., Li, Q., Liu, Y., Tang, G., 2009b. Role of mantle-derived magma in genesis of early Yanshanian granites in the Nanling Range, South China: in situ zircon Hf-O isotopic constraints. Sci. China D Earth Sci. 52, 1262–1278.

Li, X.H., Long, W.G., Li, Q.L., Liu, Y., Zheng, Y.F., Yang, Y.H., Chamberlain, K.R., Wan, D.F., Guo, C.H., Wang, X.C., Tao, H., 2010a. Penglai zircon megacrysts: A Potential new working reference material for microbeam determination of Hf-O Isotopes and U-Pb Age. Geostand. Geoanalytical Res. 34, 117–134.

Li, C., Wu, Y.W., Wang, M., Yang, H.T., 2010b. Significant progress on Pan–African and Early Paleozoic orogenic events in Qinghai–Tibet Plateau: discovery of Pan–African orogenic unconformity and Cambrian System in the Gangdese area, Tibet, China. Geological Bulletin of China 29, 1733–1736 (in Chinese with English Abstract).

Li, X.H., Tang, G.Q., Gong, B., Yang, Y.H., Hou, K.J., Hu, Z.C., Li, Q.L., Liu, Y., Li, W.X., 2013. Qinghu zircon: A working reference for microbeam analysis of U-Pb age and Hf and O isotopes. Chinese Science Bulletin 58, 4647–4654.

Li, X.H., Liu, X.M., Liu, Y.S., Su, L., Sun, W.D., Huang, H.Q., Yi, K., 2015. Accuracy of LA-ICPMS zircon U-Pb age determination: An inter-laboratory comparison. Science China: Earth Sciences 58, 1722–1730.

Li, G.-J., Wang, Q.-F., Huang, Y.-H., Gao, L., Yu, L., 2016. Petrogenesis of middle Ordovician peraluminous granites in the Baoshan block: implications for the early Paleozoic tectonic evolution along East Gondwana. Lithos 245, 76–92.

Li, S., Zhao, S., Liu, X., Cao, H., Yu, S., Li, X., Somerville, I., Yu, S., Suo, Y., 2018. Closure of the Proto-Tethys Ocean and Early Paleozoic amalgamation of microcontinental blocks in East Asia. Earth Sci. Rev. 186, 37–75.

Liang, X., Wang, G.H., Yuan, G.L., Liu, Y., 2012. Structural sequence and geochronology of the Qomo Ri accretionary complex, Central Qiangtang, Tibet: implications for the Late Triassic subduction of the Paleo-Tethys Ocean. Gondwana Research 22, 470–481.

Liang, X., Wang, G.H., Yang, B., Ran, H., Zheng, Y.L., Du, J.X., Li, L.G., 2017. Stepwise exhumation of the Triassic Lanling high-pressure metamorphic belt in Central Qiangtang, Tibet: insights from a coupled study of metamorphism, deformation, and geochronology. Tectonics 36, 652–670.

Lin, Y.-L., Yeh, M.-W., Lee, T.-Y., Chung, S.-L., Iizuka, Y., Charusiri, P., 2013. First evidence of the Cambrian basement in Upper Peninsula of Thailand and its implication for crustal and tectonic evolution of the Sibumasu terrane. Gondwana Research 24, 1031–1037.

Liu, Y., Li, C.A.I., Xie, C., Fan, J., Wu, H.A.O., 2016a. Detrital zircon U–Pb ages and Hf isotopic composition of the Ordovician Duguer quartz schist, central Tibetan Plateau: constraints on tectonic affinity and sedimentary source regions. Geological Magazine 154, 558–570.

Liu, Y.M., Li, C., Xie, C.M., Fan, J.J., Wu, H., Jiang, Q.Y., Li, X., 2016b. Cambrian granitic gneiss within the central Qiangtang terrane, Tibetan Plateau: implications for the early Palaeozoic tectonic evolution of the Gondwanan margin. Int. Geol. Rev. 58, 1043–1063.

Liu, Y.M., Li, S.Z., Santosh, M., Cao, H.H., Yu, S.Y., Wang, Y.H., Zhou, J., Zhou, Z.Z., 2019. The generation and reworking of continental crust during early Paleozoic in Gondwanan affinity terranes from the Tibet Plateau. Earth-Sci. Rev. 190, 486–497.

Miller, C., Thoni, M., Frank, W., Grasemann, B., Klotzli, U., Guntli, P., Draganits, E., 2001. The early Palaeozoic magmatic event in the Northwest Himalaya, India: source, tectonic setting and age of emplacement. Geological Magazine 138, 237–251.

Murphy, J.B., Nance, R.D., Keppie, J.D., Dostal, J., 2019. Role of Avalonia in the development of tectonic paradigms. In: Wilson, R.W., Houseman, G.A., Mccaffrey, K.J.W., Doré, A.G., Buiter, S.J.H. (Eds.), Fifty Years of the Wilson Cycle Concept in Plate Tectonics. 470, pp. 265–287 Geological Society, London, Special Publications.

O'Neil, J.R., Chappell, B.W., 1977. Oxygen and hydrogen isotope relations in the Berridale batholith. J. Geol. Soc. (London) 133, 559–571.

Peng, Z.M., Geng, Q.R., Wang, L.Q., Zhang, Z., Guan, J.L., Cong, F., Liu, S.S., 2014. Zircon U-Pb ages and Hf isotopic characteristics of Bunsumco, central Qiangtang, Qinghai-Tibet Plateau. Chin. Sci. Bull. 59 (in Chinese with English abstract), 2621–2629.

Pullen, A., Kapp, P., 2014. Mesozoic tectonic history and lithospheric structure of the Qiangtang terrane: insights from the Qiangtang metamorphic belt, central Tibet. In: Nie, J., Horton, B.K., Hoke, G.D. (Eds.), Toward an Improved Understanding of Uplift Mechanisms and the Elevation History of the Tibetan Plateau. Geological Society of America Special Paper. 507, p. 7. https://doi.org/10.1130/2014.2507(04).

Pullen, A., Kapp, P., Gehrels, G.E., Ding, L., Zhang, Q., 2011. Metamorphic rocks in central Tibet: lateral variations and implications for crustal structure. Geological Society of America Bulletin 123, 585–600.

Scrutton, R.A., 1976. Microcontinents and their significance. In: Drake, C.L. (Ed.), Geodynamics: Progress and Prospects. American Geophysical Union, Washington, D.C., pp. 177–189.

Şengör, A.M.C., 1979. Mid-Mesozoic closure of Permo-Triassic Tethys and its implications. Nature 279, 590–593.

Sláma, J., Košler, J., Condon, D.J., Crowley, J.L., Gerdes, A., Hanchar, J.M., Horstwood, M.S.A., Morris, G.A., Nasdala, L., Norberg, N., Schaltegger, U., Schoene, B., Tubrett, M.N., Whitehouse, M.J., 2008. Plešovice zircon — A new natural reference material for U–Pb and Hf isotopic microanalysis. Chemical Geology 249, 1–35.

Sun, S.S., McDonough, W.F., 1989. Chemical and isotopic systematics of oceanic basalts: implications for mantle composition and processes. In: Saunders, A.D., Norry, M.J. (Eds.), Magmatism in the Ocean Basins. London, Special Publications, Geological Society, pp. 313–345.

Tetreault, J.L., Buiter, S.J.H., 2014. Future accreted terranes: a compilation of island arcs, oceanic plateaus, submarine ridges, seamounts, and continental fragments. Solid Earth 5, 1243–1275.

Valley, J.W., Kinny, P.D., Schulze, D.J., Spicuzza, M.J., 1998. Zircon megacrysts from kimberlite: oxygen isotope variability among mantle melts. Contributions to Mineralogy and Petrology 133, 1–11.

Wang, Y., Xing, X., Cawood, P.A., Lai, S., Xia, X., Fan, W., Liu, H., Zhang, F., 2013. Petrogenesis of early Paleozoic peraluminous granite in the Sibumasu Block of SW Yunnan and diachronous accretionary orogenesis along the northern margin of Gondwana. Lithos 182-183, 67–85.

Wu, L.D., Yuan, T.Y., Jin, H.L., Liu, Y., 2018. Petrology of low-grade metamorphic quartz sandstones within northwestern Tibetan regions: implications to the tectonic evolution of the northwestern Tibet. Acta Petrologica Sinica 34, 701–718.

Xie, C.-m., Li, C., Fan, J.-j., Su, L., 2017. Ordovician sedimentation and bimodal volcanism in the Southern Qiangtang terrane of northern Tibet: Implications for the evolution of the northern Gondwana margin. Int. Geol. Rev. 59, 2078–2105.

Xu, W., Dong, Y.S., Zhang, X.Z., Deng, M.R., Zhang, L., 2016. Petrogenesis of high-Ti mafic dykes from Southern Qiangtang, Tibet: implications for a ca. 290 Ma large igneous

province related to the early Permian rifting of Gondwana. Gondwana Research 36, 410–422.
Yang, Y., Zhao, Z.B., Yuan, T.Y., Liu, Y., Li, C.Y., 2014. Ordovician parallel unconformity in Qiangtang terrane, northern Tibet: implication to Early Paleozoic evolution of northern Tibetan regions. Acta Petrologica Sinica 30, 2381–2392 (in Chinese with English abstract).
Yin, A., Harrison, T.M., 2000. Geologic evolution of the Himalayan-Tibetan orogen. Annual Review of Earth and Planetary Sciences 28, 211–280.
Zeng, L.S., Gao, L.E., 2017. Cenozoic crustal anatexis and the leucogranites in the Himalayan collisional orogenic belt. Acta Petrologica Sinica 33, 1420–1444.
Zhai, Q.-G., Zhang, R.-Y., Jahn, B.-M., Li, C., Song, S.-G., Wang, J., 2011. Triassic eclogites from central Qiangtang, northern Tibet, China: Petrology, geochronology and metamorphic P–T path. Lithos 125, 173–189.
Zhai, Q.G., Jahn, B.M., Su, L., Ernst, R.E., Wang, K.L., Zhang, R.Y., Wang, J., Tang, S.H., 2013a. SHRIMP zircon U-Pb geochronology, geochemistry and Sr-Nd-Hf isotopic compositions of a mafic dyke swarm in the Qiangtang terrane, northern Tibet and geodynamic implications. Lithos 174, 28–43.
Zhai, Q.G., Jahn, B.M., Wang, J., Su, L., Mo, X.-X., Wang, K.-l., Tang, S.-h., Lee, H.-y., 2013b. The Carboniferous ophiolite in the middle of the Qiangtang terrane, Northern Tibet: SHRIMP U–Pb dating, geochemical and Sr–Nd–Hf isotopic characteristics. Lithos 168-169, 186–199.
Zhai, Q.G., Jahn, B.M., Wang, J., Hu, P.Y., Chung, S.L., Lee, H.Y., Tang, S.H., Tang, Y., 2016. Oldest Paleo-Tethyan ophiolitic melange in the Tibetan Plateau. Geological Society of America Bulletin 128, 355–373.
Zhang, K.J., Cai, J.X., Zhang, Y.X., Zhao, T.P., 2006a. Eclogites from central Qiangtang, northern Tibet (China) and tectonic implications. Earth and Planetary Science Letters 245, 722–729.
Zhang, K.J., Zhang, Y.X., Li, B., Zhu, Y.T., Wei, R.Z., 2006b. The blueschist-bearing Qiangtang metamorphic belt (northern Tibet, China) as an in situ suture zone: Evidence from geochemical comparison with the Jinsa suture. Geology 34, 493–496.
Zhang, Z., Dong, X., Liu, F., Lin, Y., Yan, R., He, Z., Santosh, M., 2012a. The making of Gondwana: Discovery of 650Ma HP granulites from the North Lhasa, Tibet. Precambrian Research 212-213, 107–116.
Zhang, Y.-c., Shen, S.-z., Shi, G.R., Wang, Y., Yuan, D.-x., Zhang, Y.-j., 2012b. Tectonic evolution of the Qiangtang Block, northern Tibet during the Late Cisuralian (Late Early Permian): Evidence from fusuline fossil records. Palaeogeogr. Palaeoclimatol. Palaeoecol. 350-352, 139–148.
Zhang, Y.-c., Shi, G.R., Shen, S.-z., 2013. A review of Permian stratigraphy, palaeobiogeography and palaeogeography of the Qinghai–Tibet Plateau. Gondwana Research 24, 55–76.
Zhang, X.Z., Dong, Y.S., Li, C., Deng, M.R., Zhang, L., Xu, W., 2014. Silurian high-pressure granulites from Central Qiangtang, Tibet: Constraints on early Paleozoic collision along the northeastern margin of Gondwana. Earth and Planetary Science Letters 405, 39–51.
Zhang, L., Ren, Z.Y., Xia, X.P., Li, J., Zhang, Z.F., 2015. IsotopeMaker: A Matlab program for isotopic data reduction. Int. J. Mass Spectrom. 392, 118–124.
Zhang, X.Z., Dong, Y.S., Wang, Q., Dan, W., Zhang, C.F., Deng, M.R., Xu, W., Xia, X.P., Zeng, J.P., Liang, H., 2016. Carboniferous and Permian evolutionary records for the Paleo-Tethys Ocean constrained by newly discovered Xiangtaohu ophiolites from central Qiangtang, central Tibet. Tectonics 35, 1670–1686.
Zhang, X.-Z., Wang, Q., Dong, Y.-S., Zhang, C., Li, Q.-Y., Xia, X.-P., Xu, W., 2017a. High-Pressure granulite facies overprinting During the exhumation of eclogites in the Bangong-Nujiang suture zone, Central Tibet: Link to flat-slab subduction. Tectonics 36, 2918–2935.
Zhang, X.Z., Dong, Y.S., Wang, Q., Dan, W., Zhang, C.F., Xu, W., Huang, M.L., 2017b. Metamorphic records for subduction erosion and subsequent underplating processes revealed by garnet-staurolite-muscovite schists in central Qiangtang, Tibet. Geochem. Geophy. Geosyst. 18, 266–279.
Zhang, Y.X., Jin, X., Zhang, K.J., Sun, W.D., Liu, J.M., Zhou, X.Y., Yan, L.L., 2018. Newly discovered Late Triassic Baqing eclogite in central Tibet indicates an anticlockwise West-East Qiangtang collision. Scientific reports 8, 966.
Zhao, Z., Bons, P.D., Wang, G., Liu, Y., Zheng, Y., 2014. Origin and pre-Cenozoic evolution of the south Qiangtang basement, Central Tibet. Tectonophysics 623, 52–66.
Zhou, Z.G., Liu, W.C., Liang, D.Y., 2004. Discovery of the Ordovician and its basal conglomerate in the Kangmar area, southern Tibet-with a discussion of the relation of the sedimentary cover and unifying basement in the Himalayas. Geological Bulletin of China 23, 655–663 (in Chinese with English abstract).
Zhu, D.-C., Zhao, Z.-D., Niu, Y., Dilek, Y., Wang, Q., Ji, W.-H., Dong, G.-C., Sui, Q.-L., Liu, Y.-S., Yuan, H.-L., Mo, X.-X., 2012. Cambrian bimodal volcanism in the Lhasa Terrane, southern Tibet: record of an early Paleozoic Andean-type magmatic arc in the Australian proto-Tethyan margin. Chemical Geology 328, 290–308.